

IMPLEMENTATION OF FOCUSING LIGHT THROUGH HIGHLY  
SCATTERING MEDIA VIA SEQUENTIAL ALGORITHM BASED  
WAVEFRONT SHAPING

by

Desmond Kelly Williams

A thesis submitted to the faculty of The  
University of North Carolina at Charlotte  
in partial fulfillment of the requirements  
for the degree of Master of Science in  
Applied Physics.

Charlotte

2019

Approved by:

---

Dr. Rosario Porras-Aguilar

---

Dr. Donald Jacobs

---

Dr. Kosta Falaggis

©2019  
Desmond Williams  
ALL RIGHTS RESERVED

## ABSTRACT

DESMOND KELLY WILLIAMS. Implementation of Focusing Light through Highly Scattering Media via Sequential Algorithm Based Wavefront Shaping  
(Under the direction of DR. ROSARIO PORRAS-AGUILAR &  
DR. DONALD JACOBS)

Propagation of light in communications, medicine, and science is hindered by the phenomenon of optical scattering. Methods to overcome this physical limitation have and continue to be researched. This work attempts to implement the method of wavefront shaping, one of the most successful of these methods. A sequential algorithm was implemented in conjunction with a liquid crystal on silicon spatial light modulator to attempt to achieve wavefront shaping. The phase distribution was adjusted to a phase conjugate-like with the scattering media allowing increased intensity in a given region of interest at the camera plane.

## TABLE OF CONTENTS

LIST OF FIGURES	vi
CHAPTER 1: INTRODUCTION	1
CHAPTER 2: OBJECTIVES	3
2.1    Aim 1. Setup of Optical Experiment	3
2.2    Aim 2. Implementation of Imaging Through Scattering Media (Algorithms)	4
2.3    Aim 3. Trials And Troubleshooting	5
CHAPTER 3: THEORY	6
3.1.    Scattering and Diffusion	6
3.2.    Wavefront Shaping	11
3.3.    Spatial Light Modulators Based on Liquid Crystal Materials	12
3.3.1 Liquid crystals	12
3.3.2. Director Axis Reorientation	14
3.3.3 Spatial Light Modulators	15
3.4.    Algorithm for Focusing Through Scattering Media	16
3.4.1. The stepwise sequential algorithm	16
3.4.2. The continuous sequential algorithm	17
CHAPTER 4: METHODOLOGY	18
4.1    Setup Diagram	20
4.2    Setup Notes	23
4.2.1 Camera Slm Mapping	23
4.2.2 Synchronization	23

4.2.3	Camera	24
4.3	Control Program	24
4.3.1	Synchronization of SLM and Camera	25
4.3.2	Camera Parameters/Speckle Calibration	25
4.3.3	Camera SLM Mapping	27
4.3.4	Sequential Algorithm	30
4.3.5	Output	31
CHAPTER 5: RESULTS		33
5.1	Trial 1	34
5.2	Trial 2	35
5.3	Trial 3	37
CHAPTER 6: CONCLUSIONS & FUTURE WORK		40
6.1	Future Work	40
REFERENCES		42

## LIST OF FIGURES

FIGURE 1: Flowchart containing separate components of the program containing the sequential algorithm.	4
FIGURE 2: Depiction of two typical liquid crystal cells a) Planar and b) Homeotropic	14
FIGURE 3: A diagrammatic side view of a spatial light modulator, with each layer labeled in turn.	16
FIGURE 4: The stepwise sequential algorithm iterates through each index and stores the optimal phase values (represented by the red x's) individually in a separate matrix. The grey matrix represents a fully optimized phase value.	16
FIGURE 5: The stepwise continuous algorithm iterates through each index and updates to the optimal phase values (represented by the red x's) in a continuous manner.	17
FIGURE 6: A taken of the speckle pattern generated by propagating through a scattering media, in this case a piece of tape.	18
FIGURE 7: Experimental Setup to redirect light through a scattering object.	20
FIGURE 8: Operating principle of a zeroth order wave plate showing the 90 degree change in polarization of the outputted wavefront	22
FIGURE 9: Visual depiction of the operating principle of a spatial filter, showing a smooth Gaussian beam profile emerging after an unevenly distributed beam enters.	22

FIGURE 10: a) An example of a manual synchronization envelope from [6]. b) The back end of our camera with GPIO pin connector.	24
FIGURE 11: Camera Object Parameter List	25
FIGURE 12: Pictorial representation of mapping the SLM plane to the camera.	28
FIGURE 13 Flowchart for sequential continuous algorithm	31
FIGURE 14: Enhancement Factor for Run 06-05	36
FIGURE 15: a) ROI Mask(Area of Interest) b) Initial Image for Run 06-05 c) Final Image for Run 06-05	36
FIGURE 16: a) Intensity for 06-12 b) Final Image for Run 06-12	38
FIGURE 17: a) ROI Mask (Area of Interest) b) Initial Image for Run 06-12 c) Final Image for Run 06-12	38
FIGURE 18: a) (Final Image – Initial Image) Trial 06-12 b) Index Plot Trial 06-12	39

## CHAPTER 1. INTRODUCTION

Light plays an indispensable role in our day-to-day lives and in many more ways than just allowing us to see. Photonics is developing technology to generate and harness light and other forms of radiant energy whose quantum unit is the photon. Lasers, fiber optics, and electro-optical area all photonic devices prevalent in our everyday life. It is also impossible to overlook the prevalence of photonics in research settings; for scientific purposes such as optical metrology, astronomy and microscopy; and for medical purposes such as imaging, noninvasive surgical procedures and disease treatment [1, 2, 3].

Light, however does not behave the same through all different types of media. This necessitates the development of new photonic techniques in order to handle these new materials. In a transparent media like air or glass, light propagates in a straight line. In a nontransparent media, like a thick piece of paper, the physical properties of the material make it impossible for light to penetrate in the same way. On a microscopic level, the impingent electromagnetic wave is experiencing collisions with inhomogeneous irregularities within the material. These collisions cause excitations, which cause the spherical radiation of a secondary electromagnetic wave. This secondary radiation is known as scattering [4-9].

In multiple scattering samples, the incoming light is scattered successively numerous times, thereby rapidly losing the memory of the incident direction. After some scattering events, the propagation is a diffusion process. [9] When using coherent incident light from a laser, a typical interference pattern, the so-called speckle pattern, is formed in the outgoing light. This speckle pattern cannot be explained by the diffusion model of photons but is better described by a random walk of wavelets with amplitude and phase, as

in Feynman's path model. Although quantum effects are involved, they fall outside the scope of this project. Scattering and diffusion of light are huge limitations for optical imaging, but also severely hinder telecommunication, spectroscopy, and other optical techniques. In the last few decades, a tremendous effort was put in developing imaging methods that work in strongly scattering media. That research has brought forward important new photonic imaging methods like optical coherence tomography, diffusion tomography and laser speckle velocimetry.[10]

This work attempts to address the issue of imaging through scattering via successful implementation of wavefront shaping technique developed by Ivo Vellekoop, Mosk and collaborators [1]. Shaping the wavefront to match the scattering properties of the object allows us to focus light through an otherwise optically impenetrable object. While the scope of this research mainly endeavors to achieve imaging through a static object with less stringent time constraints, it's also feasible to use a similar procedure to handle dynamic and time variant media. The rest of this work will be dedicated to the following: setting down clear objectives for completion of the goals set forth; relevant theory; methodology for the experiment; results; and future work.

## CHAPTER 2. OBJECTIVES

The general objective of this research is to implement the wavefront shaping technique by means of a spatial light modulator (SLM).

To accomplish this objective, we have defined the following specific aims:

Aim 1: Setup Optical Experiment

Aim 2. Implementation of the Sequential Algorithm

Aim 3. Trials and troubleshooting

### 2.1 Aim 1. Setup of Optical Experiment

As optical systems become more complex, proper alignment becomes more challenging. [11] For example, a misaligned multi-element system will suffer from imaging errors that vary in a complex way over the field of view. In our experiment, we make adjustments to the alignment of our optical system to ensure enough power from our laser was reaching our camera plane by minimizing dissipation through our other optical elements.

In addition to that, given the importance of high precision and accuracy in our SLM-camera-computer feedback loop to appropriately update phase values to achieve enhancement it was necessary to map the SLM and camera dimensions and to spatially and temporally synchronize both devices.

Therefore, the goals expected in Aim 1 are the following,

- Optical Alignment
- Camera-SLM Mapping
- Camera-SLM Synchronization

## 2.2. Aim 2. Implementation of Imaging Through Scattering Media (Algorithms)

The proper functioning of imaging through scattering media requires to satisfy three essential tasks: i) communication with the camera, ii) communication with the SLM and iii) adequate storage of the transmission matrix [17-20]. The second aim of this work is to write a program to successfully accounts for i), ii), and iii), and executes an algorithm to redirect light through a scattering media. This work is focused on the implementation of the “sequential algorithm” described in [1, 12-17]. The previous work provides a blueprint for the necessary components and appropriate level of modularity needed for the setup to proceed ideally. A brief schema and flowchart are provided in Fig. 1 below. The sequential algorithm is the core of the redirection of light and will be described in further detail in Section 4.6.

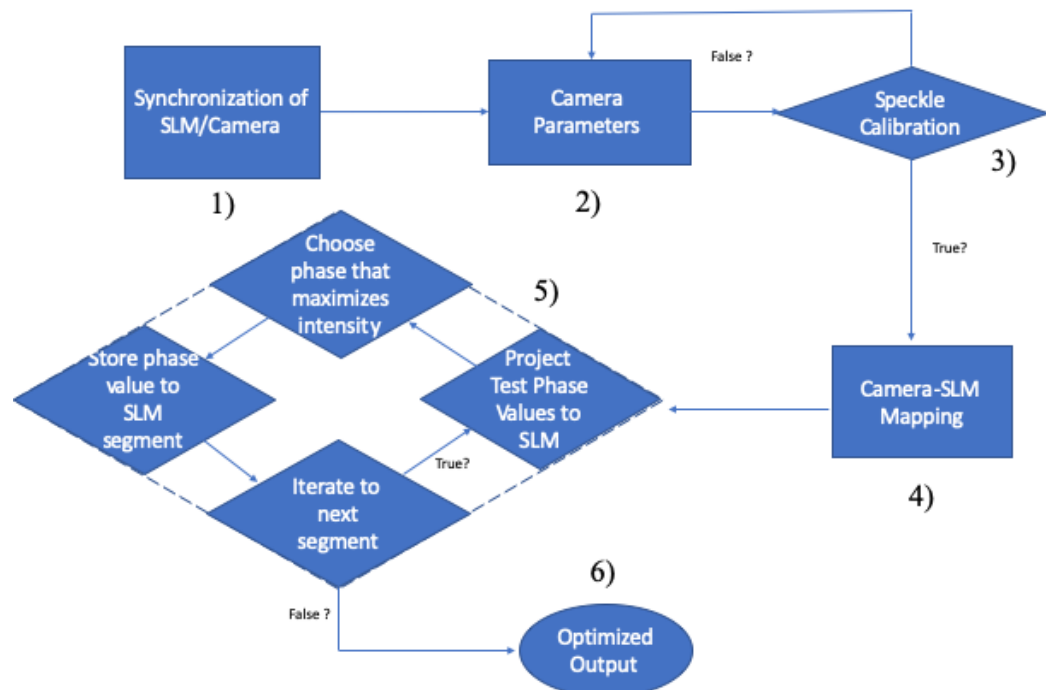


Figure 1. Flowchart containing separate components of the program containing the sequential algorithm.

The component 1) defines a delay to synchronize triggering of the camera with the adjustment and relaxation period of the SLM. The component 2) takes a test image to assure that the camera parameters such as exposure and shutter time are receiving optimal intensity data Component 3) ensures the speckle pattern generated by our scattering object is not too high in intensity to ensure the sequential algorithm is optimizing phase with usable information. Component 4) tests accurate portrayal of the SLM phase projection onto the camera. 5) Represents the continuous sequential algorithm feedback loop and 6) the qualitative and quantitative results post-optimization. We will know that Aim 2 was accomplished when light is redirected to a predefined region target in the camera (Area of Interest). The Area of Interest being, for example, 4 pixels located at center of the detector plane(camera). An increase in intensity means that light is being redirected through the scattering media towards the region of interest instead of being scattered.

### 2.3. Aim 3. Trials And Troubleshooting

The third aim in our work is to improve the performance of this setup by measuring the enhancement factor,  $\eta$ , defined by Eq. 1.

$$\eta = \frac{\langle G_i \rangle}{\langle G_0 \rangle} \quad (1)$$

where  $\langle G_i \rangle$  represents the mean gray level registered by the detector (camera) after the  $i$ -th iteration of the optimization algorithm, and  $\langle G_0 \rangle$  represents the initial mean gray level over the area of interest [13].

## CHAPTER 3. THEORY

### 3.1 Scattering And Diffusion

Our examination of the theory of scattering behavior will be conducted in the view of a plane wave impinging upon a scattering media, idealized as a slab, at an angle  $\theta_a$ . The statistical properties of wave propagation in scattering media can be understood by employing mesoscopic transport formalism [1]. The average intensity of a disordered medium can be well described by the diffusion equation [21]. In that vein we observe the behavior of light through a scattering media through the lens of diffusion theory. We follow the derivations of [21] as a useful guide for observing relevant equations.

$$I_{in}(z) = I_0 e^{\frac{-z}{l \cos \theta_a}} \quad (2)$$

The so-called Lambert-Beer Law (eq. 1) defines the decay of incoming beam through a media due to its physical characteristics, with  $l$  being the scattering mean free path and  $z$  being the propagation distance within the media,

$$l_{sc} = \frac{1}{n\sigma_{ex}} \quad (3)$$

$\theta_a$  as previously defined. Once the light has entered the slab, the diffuse intensity obeys the diffusion equation, Eq. 3:

$$\frac{\partial}{\partial t} I(\vec{r}, t) = D \nabla^2 I(\vec{r}, t) \quad (4)$$

In the steady state the time derivative vanishes, and the diffusion coefficient plays no role.

For a slab geometry there is no  $x, y$  dependence and must be solved.

$$I''(z) = 0 \quad (5)$$

With trapping plane boundary conditions, the solution is a linear function of  $z$ .

$$I(z) = I_0 \frac{L + z_0 - z}{L + 2z_0} \quad (6)$$

In the presence of absorption, the diffusion equation reads:

$$\partial_t I(\vec{r}, t) = D \nabla^2 I(\vec{r}, t) - D \kappa^2 I(\vec{r}, t) + S(\vec{r}, t), \quad (7)$$

where  $S$  is a source term, the second term on the righthand side describes absorption, and the absorption length is  $L_{\text{abs}} = 1/\kappa$ .

In a bulk system, the solution with initial conditions  $I(r, 0) = \delta(r)$  and  $S = 0$  reads

$$I(\vec{r}, t) = (4\pi Dt)^{-3/2} e^{-(r^2/4Dt) - D\kappa^2 t} \quad (8)$$

Defining the perpendicular wave vector by  $q_{\perp}$

the diffusion from point  $z$  to  $z'$  further into the media is defined as.

$$I''(z, z') = M^2 I(z, z') - \frac{S(\vec{q}_{\perp})}{D} \delta(z - z') \quad (9)$$

With the “mass”  $M$  defined by

$$M^2 = q_{\perp}^2 + \kappa^2 + i \frac{\Omega}{D} \quad (10)$$

$M$  is the inverse depth at which a given intensity contribution of an incoming beam has decayed by a factor  $1/e$ , due to spatial dephasing of the amplitudes (encoded in  $q_{\perp}$ ), temporal dephasing (expressed by  $\Omega$ ), or absorption (expressed by  $\kappa$ ).

The diffusion equation is just a wave equation with complex frequency, one sees that the solutions to the diffusion equation are a linear combination of hyperbolic sines and cosines. (The solution can also be obtained using the method of “image charges” known from electrostatics) [22].

The diffuse intensity propagator has the form [23]

$$I(z, z'; \vec{q}_{\perp}; \Omega) = \frac{\vec{S}(\vec{q}_{\perp})}{D} \frac{[\sinh Mz_{<} + Mz_0 \cosh Mz_{<}][\sinh(M)(L - z_{>}) + Mz_0 \cosh M(L - z_{>})]}{(M + M^3 z_0^2) \sinh(ML + 2M^2 z_0) \cosh ML} \quad (11)$$

The propagator describes the diffuse propagation from one point in the slab to another. With roughly equal indices of refraction inside and outside the sample, the extrapolation length  $z_0$  is a few mean free paths and thus the terms involving  $z_0$  yield contributions of order  $1/L$ . For optically thick samples ( $L \gg l$ ), this is negligible, and one has:

$$I(z, z'; \vec{q}_\perp; \Omega) = \frac{\vec{S}(\vec{q}_\perp)}{D} \frac{\sinh(Mz_<) \sinh(ML - Mz_>)}{M \sinh(ML)} \quad (12)$$

The diffuse intensity from an outside plane-wave source is assumed to be given by substituting  $z = 1$  in Eq. (11), as if all diffuse intensity originated from this  $z = 1$  plane.

Likewise, the coupling

outwards is obtained by taking  $z' = L - 1$ . In this way two extra propagators, the incoming ( $z < 0, 0 < z' < L$ ) and the outgoing ( $0 < z < L, z' < L$ ) are constructed from the internal diffusion ( $0 < z, z' < L$ ).

$$I_{curly}(\vec{r}, n) = I_{curly}(\vec{r}, \theta, \phi) \quad (13)$$

The specific intensity  $I(\mathbf{r}, \mathbf{n}) + I(\mathbf{r}, \theta, \phi)$  is defined as the radiation density emitted at position  $\mathbf{r}$  in direction  $\mathbf{n} = (\sin \theta \cos \phi, \sin \theta \sin \phi, \cos \theta)$  in a system with density  $n$  of scatterers. Let  $dU$  be the radiation energy in a given frequency interval ( $\omega - 1/2 \Delta\omega, \omega + 1/2 \Delta\omega$ ), transported through a surface  $d\sigma$  in directions lying within a solid angle  $d\mathbf{n}$  centered on  $\mathbf{n}$ , during a time interval  $dt$ . This energy is related to the specific intensity as [24]

$$dU = I_{curly} \cos \Theta \Delta\omega d\sigma d\mathbf{n} dt \quad (14)$$

where  $\Theta$  is the angle between the director  $\mathbf{n}$  of the emitted radiation and the normal of  $d\sigma$ .

The energy depends in general on the position  $\mathbf{r} = (x, y, z)$ , the direction  $\mathbf{n}$ , the frequency  $\omega$ , and the time  $t$ .

$$dI_{curly} = -n\sigma_{ex} I_{curly} d\sigma \quad (15)$$

If the radiation propagates over a distance  $ds$  there is a loss of intensity to scattering into other directions due to absorption. There is also a gain term denoted by the so-called Source Function:

$$J_{curly}(r, \theta, \phi) = \int_0^\pi \int_{-\pi}^\pi p(\theta, \phi; \theta', \phi') \frac{\sin \theta' d\phi'}{4\pi} I_{curly}(\vec{r}, \theta', \phi') \quad (16)$$

The radiative-transfer equation expresses the net effect of the gain-loss mechanism and the loss term  $-I$  leads to the Lambert-Beer law with scattering mean free path denoted by:

$$\frac{1}{n\sigma_e x} \frac{dI_{curly}}{ds} = J_{curly} - I_{curly} \quad (17)$$

Unscattered intensity decays exponentially as a function of the distance from the source. The characteristic distance between two scattering events is the scattering mean free path. If the scattering is weak, the radiation direction has not changed all that much. The diffusion constant must then be large. In other words, the factor  $l$  in the identity  $D = 1/3 v l$  cannot be the scattering mean free path. One expects that  $l$  is the distance over which the direction of radiation gets lost. This length scale is called the transport mean free path. The time dependent radiative transfer equation reads:

$$t_{sc} \frac{\partial}{\partial t} I_{curly}(\vec{r}, \vec{n}, t) + l_{sc} \vec{n} \cdot \nabla I_{curly}(\vec{r}, \vec{n}, t) = \int \frac{d\vec{n}'}{4\pi} p(\vec{n}, \vec{n}') I_{curly}(\vec{r}, \vec{n}', t) - I_{curly}(\vec{r}, \vec{n}, t) \quad (18)$$

with radiation density  $I$

$$I(\vec{r}, t) = \int d\vec{n} I_{curly}(\vec{r}, \vec{n}, t) \quad (19)$$

and local current density  $J$

$$\vec{J}(\vec{r}, t) = \frac{l_{sc}}{t_{sc} c} \int d\vec{n} I_{curly}(\vec{r}, \vec{n}, t) \vec{n} \quad (20)$$

Integrating the above we get the Continuity Equation:

$$\partial_t I(\vec{r}, t) + \nabla \cdot \vec{J}(\vec{r}, t) = -\frac{1-a}{t_{sc}} I(\vec{r}, t) \quad (21)$$

If a process changes slowly in time we find:

$$\vec{J}(\vec{r}, t) = -D \nabla I(\vec{r}, t) \quad (22)$$

Insert into the continuity equation and get,

$$\partial_t I(\vec{r}, t) = D \nabla^2 I(\vec{r}, t) - \frac{1-a}{t_{sc}} I(\vec{r}, t) = D \nabla^2 I(\vec{r}, t) - D \kappa^2 I(\vec{r}, t) \quad (23)$$

which again is the diffusion equation with:

$$D = \frac{t_{sc}^2}{3t_{sc}(1 - \langle \cos \Theta \rangle)} = \frac{1}{3} v l_{tr} \quad (24)$$

Dorokhov predicted a striking multichannel interference effect. Using random matrix Dorokhov showed that light passing through a semi-opaque material does so by traveling through a small number of open eigenchannels corresponding to a linear combination of free modes that have a transmission coefficient of close to unity [25,26]. Waves coupled to an open channel will be fully transmitted through a disordered media, regardless of optical thickness. Most of the power is diffusely reflected in transport because most modes of an incident plane wave couple to closed eigenchannels with a transmission coefficient of close to zero. The diffusion equation is of the Sturm-Liouville type so its eigenfunctions form a complete and orthogonal set [9,27].

Multiplying the energy density at a point in space and multiplying by its velocity results in intensity, with a resulting unit of power divided by area.[28] We use our

$$E_{\alpha}^{opt,\beta} = (T_{\beta})^{\frac{1}{2}} t_{\beta\alpha}^* \quad T_{\beta} = \sum_{\alpha}^N |t_{\beta\alpha}|^2 \quad (25)$$

algorithm to maximize intensity in one of the transmitted free modes, corresponding to a single diffraction limited spot. This mode is labeled with the index beta. The ideally shaped

incident wave front for maximizing the intensity in beta is given by

Where  $T_\beta$  normalizes the total incident power. Intensity is a property of anything that can transmit energy. For a monochromatic plane wave or Gaussian beam if  $E$  is the complex amplitude to the electric field, the time-averaged energy density is given:

$$\langle U \rangle = \frac{n^2 \epsilon_0}{2} |E|^2 \quad (26)$$

and the intensity in a local region is obtained by multiplying this expression by the wave velocity,  $c/n$ : where  $n$  is the refractive index,  $c$  is the speed of light in vacuum and  $\epsilon_0$  is the vacuum permittivity.

$$I = \frac{cn\epsilon_0}{2} |E|^2 \quad (27)$$

### 3.2 Wavefront Shaping

In the phase optimization algorithm, we assume that the incident light homogeneously illuminates the modulator and all input channels carry the same intensity. The goal is to focus the light on a single spot, i.e., strengthen a single output channel. We are only interested in focusing light to a single spot, so we only consider a single transmission channel,  $E_m$ . The intensity transmitted into channel  $m$  is given by

$$|E_m|^2 = \frac{1}{N} \left| \sum_n^N t_{mn} e^{i\phi_n} \right|^2 \quad (28)$$

In order to achieve wavefront shaping it is necessary i) to possess a device that can modulate incoming waves either in amplitude-or phase, and ii) to develop an algorithm to optimize the amplitude/phase distribution in such device (see Section 3.4).

A broad range of these devices exist including Spatial Light Modulators (see Section 3.3), Deformable Mirrors, and Digital Micrometer devices. Each of these devices have their own positives and negatives dependent upon what kind of modulation the

experiment requires.

Of the three options, for this experiment we have chosen to use a Spatial Light Modulator as our modulation device. Our goal is to achieve wavefront shaping by optimizing phase addressable segments on our device. As such the device that allows to maximize the number of phase addressable elements is the optimal choice. While the deformable mirror could be faster and potentially equal in cost, it is unable to match the sheer size of phase addressable elements present in a Holoeye Pluto- 1920 x 1080-pixel Spatial Light Modulator (SLM). This SLM is based on the voltage-controllable birefringence of liquid crystal molecules that will be discussed in Section 3.3.

### 3.3. Spatial Light Modulators Based On Liquid Crystal Materials

#### 3.3.1 Liquid crystals

In addition to the solid crystalline and liquid phases liquid crystals have unique intermediate phases with the physical characteristics of both a liquid and a crystal. These materials are known as mesogens and their phases are known as mesophases. [31,32] Lyotropics, thermotropics, polymeric, are the most widely studied mesogens.[33] The many liquid crystal mesophases, nematic, cholesteric, smectic, and ferroelectric, are highly dependent on constituents, substituents, concentration, and temperature. The Holoeye Pluto-2 phase-only spatial light modulator used in this experiment possesses a vertically aligned nematic liquid crystal cluster.

In general, nematic molecules exhibit centrosymmetry; their physical properties are the same in the  $+n$  and the  $-n$  directions. [33] In other words, they assemble such that their bulk magnetic dipole moment vanishes if the individual molecules carry a permanent electric dipole.

The spontaneous electric polarization  $\mathbf{p}$  is a vector and represents a breakdown of symmetry, meaning it has a directional preference. If  $\mathbf{P}$  exists, it must be locally perpendicular to  $\mathbf{n}$  if the liquid crystal properties are independent of the director axis  $\mathbf{n}$  direction. An aligned sample may thus be regarded as a single crystal, in which the molecules are, on the average, aligned along the direction defined by the director axis  $\mathbf{n}(\mathbf{r})$ . [32]

Liquid crystal molecules are viewed as rigid rods; their entire collective behavior may be described in terms of the director axis  $\mathbf{n}(\mathbf{r})$ , a vector field. In other words, in a spatially “distorted” nematic crystal, the local optical properties are still those pertaining to a uniaxial crystal and remain unchanged; it is only the orientation (direction) of  $\mathbf{n}$  that varies spatially. For nematics, the states corresponding to  $-\mathbf{n}$  and  $+\mathbf{n}$  are indistinguishable. In other words, even if the individual molecules possess permanent dipoles (actually most liquid crystal molecules do), the molecules are collectively arranged in such a way that the net dipole moment is vanishingly small; that is, there are just as many dipoles up as there are dipoles down in the collection of molecules represented by  $\mathbf{n}$ . [32]

### 3.3.2. Director Axis Reorientation

As an illustration, consider the two typical nematic liquid crystal cells as depicted in Figure 2 below

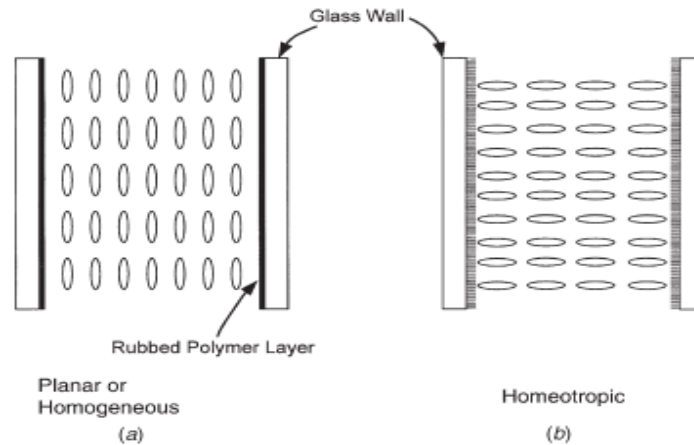


Figure 2. Depiction of two typical liquid crystal cells a) Planar and b) Homeotropic[32]

in which the director axis is aligned in the homogeneous (or planar) and homeotropic states. For electro-optic application, the cell windows are typically coated with a transparent conductor such as indium tin oxide (ITO) to allow the application of an electric voltage (field) across the cell. In general, ac voltages are employed to avoid current flows, liquid crystal orientation instabilities, heating, and other electrochemical effects associated with a large dc field that will degrade the liquid crystals. The response of the nematic liquid director axis to the applied field depends on the dielectric anisotropy. [34]

For positive uniaxial liquid crystal molecules, the director axis will tend to align along the electric field, whereas in negative uniaxial liquid crystals, the director axis will tilt away from the electric field. To produce field induced director axis reorientation, one would employ positive uniaxial nematic liquid crystal in planar alignment and negative uniaxial nematic liquid crystal in homeotropic alignment. In the latter case, since the

molecules are free to rotate in any (random in fact) direction away from the homeotropic state, usually some small pretilt is imparted on the cell surface to “guide” the molecular reorientation towards the pretilt direction when the field is applied. It is important to bear in mind that the real liquid crystals in practical use are usually not single constituents or purely dielectric.

Since the dielectric anisotropy is frequency dependent, one could create a dual-frequency liquid crystal (DFLC) that is a mixture of liquid crystals with different dielectric dispersions. This DF LC possesses an effective positive anisotropy at one ac field frequency, but a negative anisotropy at another frequency. In that case, a planar aligned cell, for example, could be switched to and from the homeotropic alignment state by switching the frequency of the applied field. [32,34] Since the response times of the director axis are dependent on the applied voltage, DF LC could allow one to switch between the two alignment states at a faster rate than the director axis’s natural (no voltage applied) relaxation time.

### 3.3.3 Spatial Light Modulators

The most popular types of light modulators usually use liquid crystal displays because of their high number of degrees of freedom, and high optical efficiency. [35] In our experiment, light is modulated with a twisted nematic (TN) liquid crystal display. This LCD can modulate light at a refresh rate of 60 Hz at a resolution of 1920 x 1080 pixels and an 8  $\mu\text{m}$  pixel pitch leading to a 0.7” active area diagonal with an aspect ratio of 16:9

The operating principle of LCDs is based on the birefringence of rod-like liquid crystal molecules. A transmissive liquid crystal is stacked within a cross polarizer system. The helical liquid crystal structure changes the polarization angle of the incident light to transmit light through the second polarizer. Applying a voltage over the LCD cell aligns the liquid crystal molecules with the electric field.

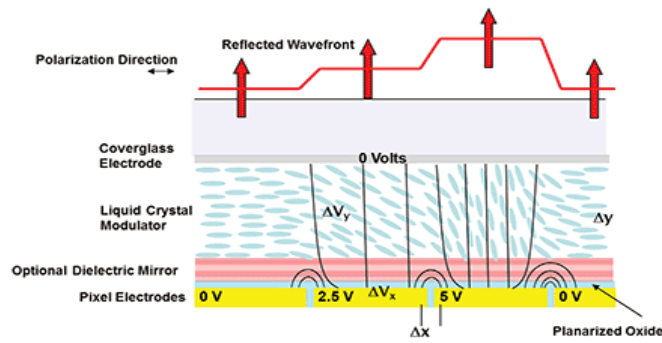


Figure 3. A diagrammatic side view of a spatial light modulator, with each layer labeled in turn.[42]

### 3.4 Algorithm For Focusing Through Scattering Media

#### 3.4.1. The Stepwise Sequential Algorithm

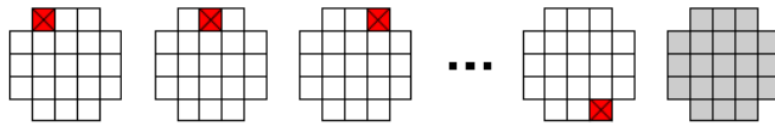


Figure 4. The stepwise sequential algorithm iterates through each index and stores the optimal phase values (represented by the red x's) individually in a separate matrix. The grey matrix represents a fully optimized phase value.[1]

When the phase of one or more segments of our SLM is changed, the target intensity has a sinusoidal response. We operate the phase modulator at 60 Hz in our experiments and take ten measurements for each iteration, with iterations being defined by  $N$ ; we have  $T_i \approx 1.6s$ . However, when  $N \cdot T_i \gg T_p$ , the speckle pattern decorrelates before all measurements are performed and the algorithm will not work. Fig. 8 depicts the operative

schema for the stepwise sequential algorithm.

$T_i$  = Iteration time

$T_p$  = Persistence time of the material

### 3.4.2. The Continuous Sequential Algorithm

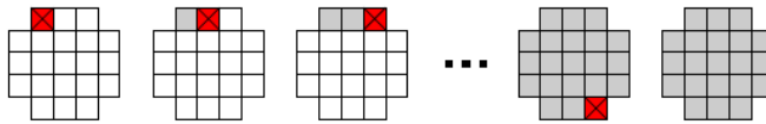


Figure 5. The stepwise continuous algorithm iterates through each index and updates to the optimal phase values (represented by the red x's) in a continuous manner.[1]

The continuous sequential algorithm is very similar to the stepwise sequential algorithm except for the fact that the phase of each segment is set to its optimal value directly after each measurement. This approach has two advantages over the sequential algorithm: the algorithm runs continuously follows dynamic changes in the sample's scattering behavior; furthermore, the target intensity signal starts to increase directly, which decreases noise in successive measurements. It is still necessary to adjust  $N$  to the persistence time  $T_p$ . Fig. 5 depicts the operative schema for the stepwise sequential algorithm. This algorithm does not guarantee to reach the local maximum.

## CHAPTER 4. METHODOLOGY

Using Huygens principle, wave propagation in a disordered medium can be examined insightfully [1]. When an incident beam of light hits a small particle in an object, some of the light is scattered and forms a spherical wave moving away from the particle. This spherical wave hits other particles, giving rise to a growing number of interacting waves. Light propagation in a disordered scattering medium is extremely complex; light is typically scattered hundreds or thousands of times before it reaches the other side of the sample. This forms a complicated chaotic intensity correlation pattern, that is the result of the interference of many different waves. When this pattern is caused by a coherent source it is known as speckle [8]. An example of a speckle pattern is shown in Fig. 6 below.

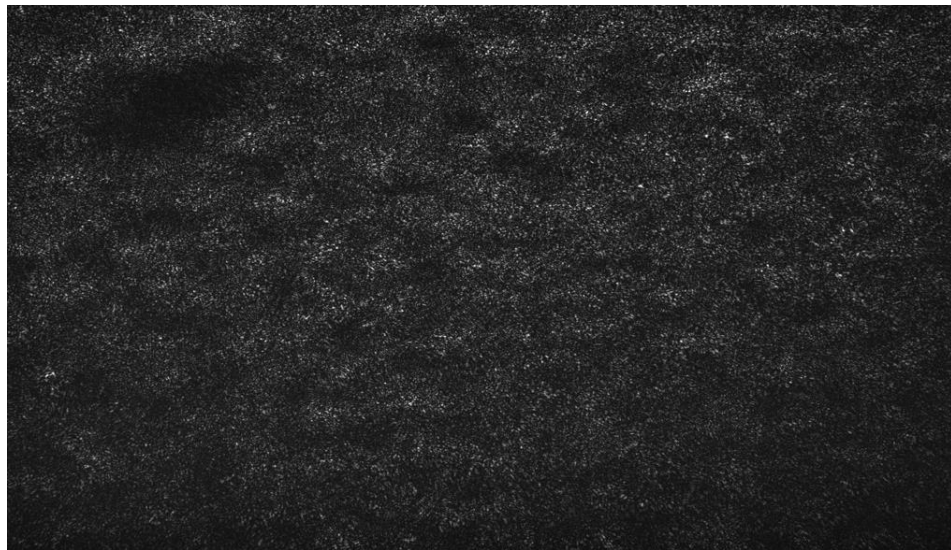


Figure 6. A taken of the speckle pattern generated by propagating through a scattering media, in this case a piece of tape

The random intensity distribution known as a speckle pattern is formed when

coherent light either is reflected from a rough surface or propagates through a medium with random refractive index fluctuations. Such patterns are clearly visible even to the casual observer when highly coherent laser light is used. In general, the statistical properties of speckle patterns depend both on the detailed properties of the random surface or medium and the coherence of the incident light, although for perfectly coherent light this dependence on the random scatterer is almost negligible if the scatterer introduces path differences greater than one wavelength[6]. The behavior and appearance of the speckle pattern within a scatterer can be described by its transmission matrix. The transmission matrix (TM) of a scattering medium characterizes the relationship between the output modes and the input modes. Therefore, once the TM of a scattering medium is acquired, the incident object waves can be reconstructed from the distorted transmitted waves [17]. A transmission matrix for the specific sample can be characterized and then reconstructed, meaning not necessarily for each individual scatterer within the media, but their conglomeration, as the eigenfunctions of the diffusion equation are for transmission through the eigenchannels of the media.

If we consider the large number of elements of the TM each as an individual light beam the premise of the experiment becomes clear. We illuminate the opaque object with thousands of light beams, instead of one. Each of these beams form a different random speckle pattern when it is scattered. The total light field at a given point behind the scattering sample is the sum of the speckle patterns of all incident beams. Since the object is disordered, each beam contributes to the field with a random phase. Therefore, the contributions from different beams interfere in such a way that they cancel each other out [1]. Next, a spatial light modulator delays in time each of the beams of the incident light

relative to the others and thereby shapes the wavefront. The algorithm then redirects light in a sequential manner towards the area of interest.

As mentioned earlier, a computer-controlled algorithm optimizes the intensity in a single point. It does this by changing the phase of the beams one by one, until their speckle patterns all interfere constructively in phase at the target. All contributions interfere constructively in the target and the intensity in the Region of Interest increases dramatically. The wavefront has been redirected. This procedure can be accomplished to redirect light into a single pixel in the camera or in to a region outside the optical axis. When the microscopic scatterers in the object move, such as the possible result of vibrations, a completely different wavefront is required. Given the low frequency response of the SLM (60 Hz), this method works for static scatterers. However, this implementation has been used to provide proof of concept of wavefront shaping through static scattering objects [1,12].

#### 4.1 Setup Diagram

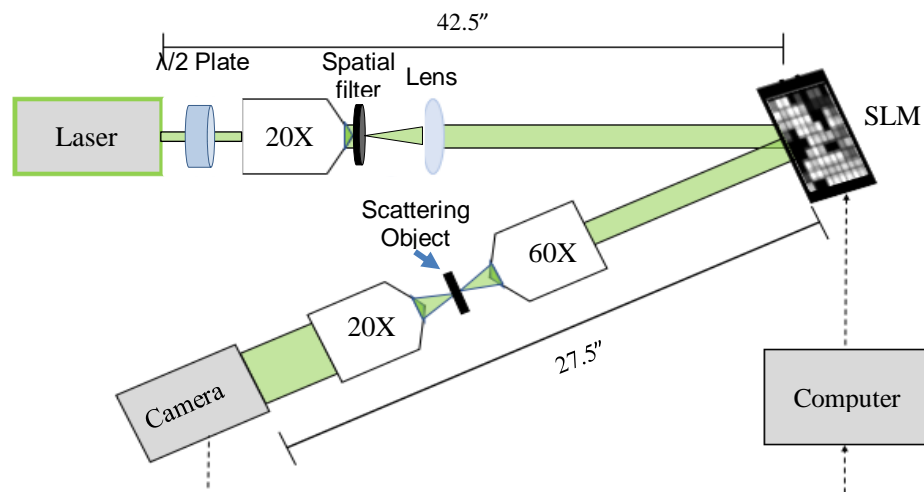


Figure 7. Experimental Setup to redirect light through a scattering object.

Fig. 4 depicts the experimental setup. We use an Obis Coherent 532nm laser beam through a  $\lambda/2$  Plate (to assure a correct polarization to align with the fast axis of our SLM) and then through an objective, spatial filter, and a lens to assure a collimated beam. The beam then illuminates a reflective SLM Holoeye Pluto-2, at an approximate 8 degree incidence. This illumination angle is required to ensure that the SLM does not modify the polarization state of the light. The reflected light then propagates through a 60X imaging objective, through our scattering media, into a 20X magnifying objective and onto the camera (FLIR Point Grey Flea3 L3-GE-50S5M). The camera is connected via a GiGE cable into our computer which will host and run the MATLAB implemented sequential algorithm which updates our SLM.

#### SETUP COMPONENTS:

##### Spatial Light Modulator

Holoeye Pluto-2 Spatial Light Modulator

1920 x 1080 Device Resolution

8 $\mu$ m pixel size

##### Camera CCD

FLIR Point Grey Flea3

FL3-GE-50S5M

2448x2048 Resolution

GigE(Gigabit Ethernet) Connection

Bus Speed S1600

##### Light Source

Controllable Coherent OBIS LS 532-20 [36]

Coherent OBIS heatsink

Relevant Optical Components

Thorlabs  $\lambda/2$  @532nm Zeroth

Order Wave plate

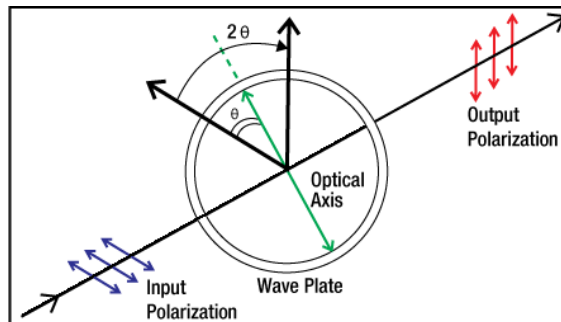


Figure 8. Operating principle of a zeroth order wave plate showing the 90 degree change in polarization of the outputted wavefront.

Spatial Filter (20X Objective lens with a 12.5 micron pinhole)

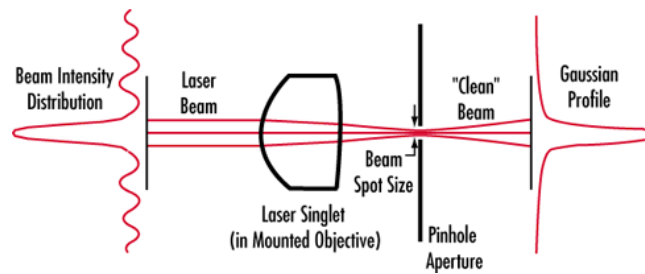


Figure 9. Visual depiction of the operating principle of a spatial filter, showing a smooth Gaussian beam profile emerging after an unevenly distributed beam enters.

## 4.2. Setup Notes

### 4.2.1 Camera SLM Mapping

The primary driver of the focusing procedure is the information generated by the phase adjustment of the SLM; as such, it was necessary to ensure proper dimensional mapping from the SLM to the CCD. [1] presented a helpful guide. "The procedure for mapping between the CCD and the SLM. (a) A mask was placed at the symmetry plane of the SLM. The mask was illuminated and imaged on CCD 1. (b), a phase pattern was displaced on the SLM, which was imaged on CCD 2. (c) The mask was illuminated and was imaged on CCD 2. The exception to the scheme used here was that only a single CCD was used.

### 4.2.2 Synchronization

In order to properly run our algorithm, the PC must be getting the most recent and complete phase information, which means that our camera must be capturing it. However, the SLM has a refresh rate (60 Hz) that has to be synchronized with the camera timing for proper detection. To that end, before running our sequential algorithm the camera has to be synched to the SLM via an RCX cable, to assure that the camera was triggering during a stable SLM state, and with the lowest possible latency time between shutters. Fig 7a. taken from [1] accurately depicts what the RCX cable is achieving automatically as opposed to what they manually programmed.

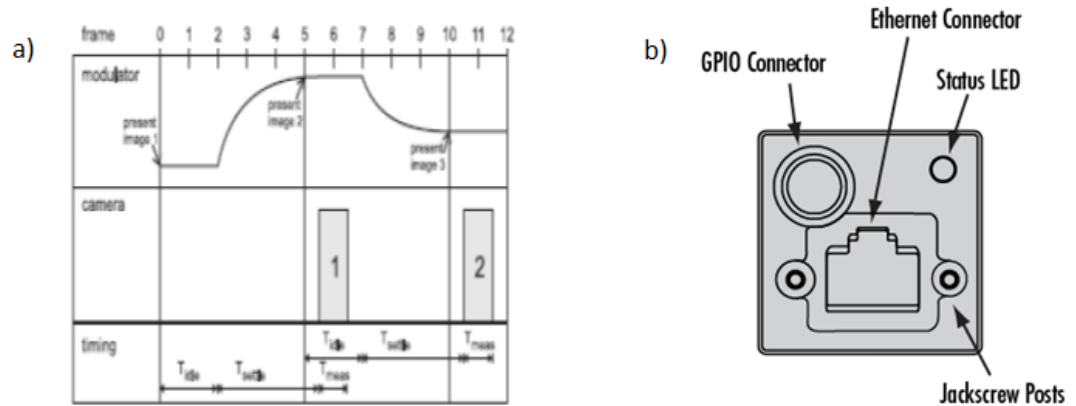


Figure 10. a) An example of a manual synchronization envelope from [6]. b) The back end of our camera with GPIO pin connector.

Our experiment was synchronized via software. This was accomplished by adding a time delay between the phase display and image capture process (SLM and CCD).

#### 4.2.3 Camera

In order to communicate with the camera through the CCD's high throughput GigE [28] port it was necessary to learn more about the firmware and triggering mechanisms within the camera [28]. As our primary software was MATLAB, we made use of the already installed Image Acquisition Package. Within the Image Acquisition Package adaptors for our specific camera hardware were downloaded. With these steps completed we were able to successfully create a camera object and change camera parameters within MATLAB.

#### 4.3. Control Program

The control program for the experiment was run as a single script in MATLAB instead of separate functions in order to improve succinctness and usability. However, the organization of the script categorically follows the flowchart/schema presented in chapter 2. Each part of the program is essentially one separate component within the schema, i.e.

(Camera Parameters, Camera-SLM Mapping, Sequential, etc.). The following section is dedicated to explaining the relevant variables and their function within each component.

#### 4.3.1 Synchronization of SLM and Camera

We use the **TimerTest()** script in order to adequately synchronize the camera triggering and SLM phase-update process. **TimerTest()** has an input of several stock images of black numbers on a blank background. To test the appropriate delay between

Display Summary for Video Source Object:

```

General Settings:
  Parent = [1x1 videoinput]
  Selected = on
  SourceName = Default
  Tag = [0x0 string]
  Type = videosource

Device Specific Properties:
  Brightness = 0
  Exposure = -0.75
  ExposureMode = Manual
  FrameRate = 25
  FrameRateMode = Auto
  Gain = 2.4282
  GainMode = Manual
  Gamma = 1
  GammaMode = Manual
  PacketDelay = 400
  PacketSize = 1486
  SerialNumber = 18085734
  Sharpness = 1024
  SharpnessMode = Manual
  Shutter = 38.7932
  ShutterMode = Auto
  Strobe1 = Off
  Strobe1Delay = 0
  Strobe1Duration = 0
  Strobe1Polarity = Low
  Strobe2 = Off
  Strobe2Delay = 0
  Strobe2Duration = 0
  Strobe2Polarity = Low
  Strobe3 = Off
  Strobe3Delay = 0
  Strobe3Duration = 0
  Strobe3Polarity = Low
  Temperature = 325.9
  TriggerDelay = 0
  TriggerDelayMode = Manual

```

Figure 11. Camera object Parameter List

phase change and camera trigger, we utilize the **pause(t)** function built in to MATLAB. We the numbers 1-5 in sequence on our SLM, and then trigger the camera after each number is projected. We then see how clear the phase image is reconstructed on our camera. If the image corresponding to the trigger number is unclear or displays the phase reconstruction of a past number i.e.(capturing the number 1 on trigger 2) than we know the trigger delay is too short, and the value of **t** should be higher. A delay time of 150ms was found to be the optimal delay time to facilitate up-to-date phase information. This **t** value was used as a parameter any time the phase needed to be updated within the sequential algorithm.

#### 4.3.2 Camera Parameters/Speckle Calibration

The program opens by making a video object within MATLAB with our camera. The addressable video object can be created from a number of camera specific modes of various resolutions,

in our case the 2448 x 2048 pixel mode was chosen to maximize surface area and resolution at the focal plane. We then define a finer area of interest (400 x 400 pixels) to focus our phase optimization process. Before the experiment can begin appropriately, it is necessary to ensure the image of the received speckle pattern will be acceptable to run our sequential algorithm. This means the intensity( average gray level) must be within a tolerable threshold value (roughly greater than 20, less than 35): bright enough to appropriately glean information and update the algorithm; dim enough not to saturate the camera and still be able to witness an appreciable change in intensity as the phase is optimized. Our camera has built in parameters which allow it to automatically try and maximize the brightness of the received image, which need to be appropriately adjusted in order to obtain our tolerable intensity value. A list of these parameters are shown in Fig. 10.

In our case, we leave most of the available parameters untouched from their default values, but manually set the optically relevant ones: Brightness, Exposure, Gain, Gamma, and Sharpness. Gamma controls the black/white contrast in our image and so we set it to unity, as we need to witness the contrast in order to get complete information about our speckle pattern. Sharpness is a measure of clarity of the received image, so by default we set it to 1024 to maximize resolution. Gain, exposure, and brightness are all parameters which either raise or lower the intensity of our image in time (exposure is the amount of light gathered in a unit time) or in space (both, gain and brightness physically amplify or dampen the received waveform once it's received in the camera). Within our program we manually set Gain to 1 and brightness to zero. With these parameters set, we focus mainly on changing the Exposure in order to achieve a threshold intensity to allow for an improvement while redirecting light with the SLM.

For this purpose, the program runs **exposureCheck(exposureValue)**, this function takes in an exposure value (set to 2.25 near the maximum) and runs a conditional statement which progressively lowers the value by .25 until the intensity is within our acceptable region. It does this by taking an image at a given exposure value, converting the entire 400 x 400 pixel region into a 1 dimensional vector, and taking the mean gray level of that vector. If the mean gray level is higher than 35 the exposure is lowered, and the process begins over again. Once our exposure is set to an appropriate value (in Trial 3's case 0.75), we output the attained mean grey level value and set our video objects exposure time.

#### 4.3.3. Camera SLM Mapping

Once assured that the SLM will accurately synchronize with the camera in time, it must be assured the phase objects projected to it are accurately represented in space; that is, whatever phase we project onto the SLM will be projected where we expect on the camera. Macroscopically, part of this is due to alignment of the system, but within the sequential algorithm there are several different matrices that should align properly with each other, both in size and position to avoid data loss and dimension mismatch errors. For example, if the applied 0 gray level(black) padding for the variable **phase3** does not adequately reflect the available pixel space on the SLM, its possible our optimization region will not be projected where expected.

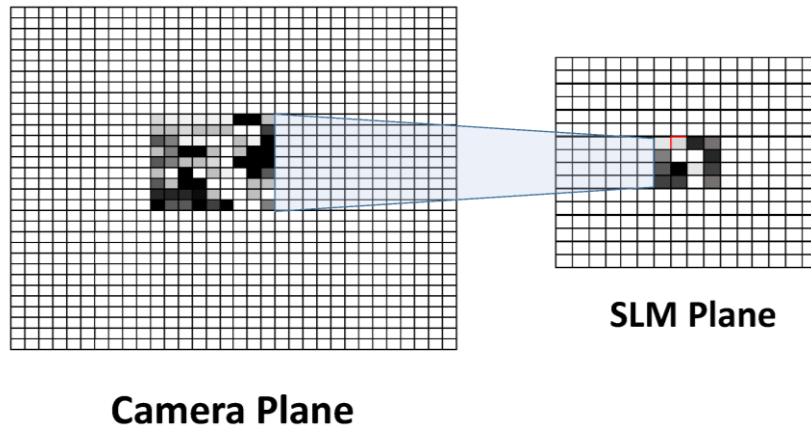


Figure 12. Pictorial representation of mapping the SLM plane to the camera

In order to physically send the phase values to the SLM we make use of the Holoeye SDK (Software Development Kit). Using the SDK has various benefits over a MATLAB specific function. The first and most important is ensured accurate representation. Using the SDK gives access to the SLM's actual data buffer, so as opposed to merely seeing what's projected **onto** the SLM plane, we can see exactly the phase data being sent. This adds a layer of additional user feedback to ensure everything is running smoothly on the hardware level. Secondly, using the SDK allows the user to project a preview of the SLM on screen, as opposed to everything happening off-screen via the second projected monitor. By projecting the SLM on-screen progress can be closely monitored during the phase updating procedure. In addition, previewing the screen this way lets you monitor progress without potentially affecting the phase optimization process by simply moving your mouse or accidentally moving a window on to the second monitor. In this way it also adds a layer of stability.

Initially we specify the variable **N**, which is the active number of pixels to be utilized on our 1920 x 1080 SLM. The variable **updatePosition** allows us to specify our Area of Interest for phase optimization within the 400 x 400 pixel box we have designated

as the Region of Interest (on our camera. This designated area is where the intensity will be measured and compared for phase update. The variable **updateRegion** fills out the rest of our ROI with a 0 gray level padding to create our phase mask for optimization. The indices of the Area of Interest are saved in the variables **cx** and **cy** to be used in the sequential algorithm to check for intensity. The variable **holdingImages** is a 400 x 400 matrix of which the third dimension will eventually store the images generated from each iteration of the sequential algorithm. We define how large the phase addressable segments of the **N** pixels of our SLM will be with the variable **segmentSize**. Varying **segmentSize** lets us define the level of precision we want in our phase updating process. Segment size is inversely proportional achievable higher enhancement factor.

By decreasing the segment size, we increase the phase addressable regions, thus increasing our possible enhancement factor. For example if we designate **N** to be 512 pixels and **segmentSize** to be 16, we end up with 1024 phase addressable segments, corresponding to 1024 iterations within the sequential algorithm. **phase2** is an empty matrix to hold our phase in through the updating process, while **phase3** is the matrix which actually gets updated continuously to the optimal phase values once each segment is properly optimized.

The variable **call** stores the initial phase values of comparison within the sequential algorithm. Using **call** lets us accurately map our SLM plane to our camera. It has size **N x N**, but its location is specifically the area on the camera where the SLM phase optimization should occur. **call** is effectively our targeting variable. As previously stated, alignment macroscopically addresses our Camera-SLM mapping, but it is possible the projection plane of the SLM is slightly off center. In this case it is necessary to “steer” our

SLM screen by adding an offset to **call** which precipitates an offset in the padding around **phase3** when sent to the SLM. In this way we can microscopically adjust for any small errors incurred during alignment to ensure maximum precision. This is another instance where being able to preview the SLM on screen via the SDK proves tremendously beneficial.

#### 4.3.4 Sequential Algorithm

The sequential algorithm represents the core of our control program. We implemented the sequential continuous algorithm, as introduced in Chapter 2 . We initialize a for loop from 1 : **total**, with **total** representing the total number of iterations (phase addressable segments). There are two counting variables **mm** and **nn**, which count the row and column indices of the current segment respectively and are incremented at the end of the loop. A nested for loop iterates  $j = 1:10$  representing 10 different phase values  $j*25(10-250)$ . Within each loop the phase value is adjusted, stored in **phase2**, then sent to **phase3** for projection onto the SLM.

Once **phase3** is adjusted it is sent via the SDK **heds\_show\_phasevalues(phaseData)** function to the SLM. A snapshot is taken and the intensity in the Area of Interest stored in a temporary

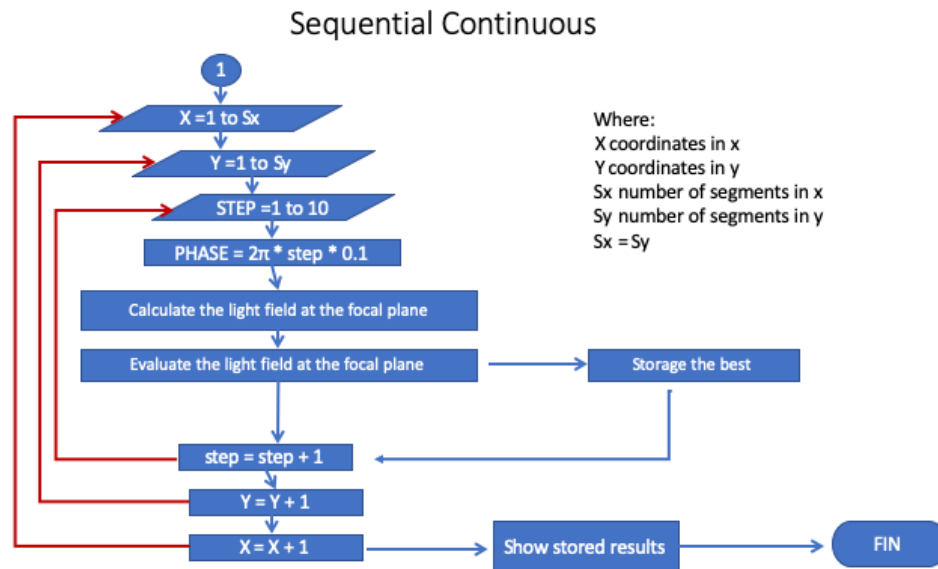


Figure 13. Flowchart for sequential continuous algorithm

holding variable. Exiting the nested for loop each of the 10 intensity values are analyzed, and the highest is stored in the variable **val. phase2** then updates the segment with the phase value corresponding to the max found in **val. phase2** is again sent to **phase3** which is projected permanently onto that specific segment for the duration of the run. A snapshot is taken, stored in the variable **XX** and our intensity is plotted for that iteration. All counting variables are incremented and the for loop begins anew.

#### 4.3.5 Output

Quantitatively our expected output will be 2 graphs; an intensity in the Area of Interest vs time graph, and an Enhancement factor (Mean Gray Level(initial)/MGL(iteration)) vs time(iteration number) graph. Each of these graphs will be plotting data from a vector of size **total** whose elements can be analyzed on their own. To quantitatively assess the level of transmission achieved, an image will be taken after the last iteration to view the final results of the phase optimization. In addition, the holding

variable **XX** stores snapshots from each of the **total** iterations, which can be examined individually, or to compile in a video to witness progressive improvement.

## CHAPTER 5. RESULTS

The primary objective of this work was to achieve focusing through highly scattering media via sequential algorithm based wavefront shaping. Its success was measured in several ways. The first small achievement was in the successful implementation of a complex, experimental setup achieving seamless integration of analog and digital optical equipment, as well as digital components. The next measure of success was the degree to which this work was successfully able to image through our scattering media. Our goal was to see iteration by iteration improvement of enhancement factor [13].

It is predicted from previous works [13] that a plateau in enhancement factor gains will be reached upon a certain number of iterations. This saturation varies based on the number of segments of the SLM used to optimize the phase of our transmission matrix. We achieved focusing at multiple segmentations and compared the results to previous implementations of similar experiments. Qualitatively we captured a final image post trial that displays obvious intensity enhancements over background noise, indicated by a much brighter spot where light has been focused on a dark background where scattering has diffused light propagation.

The course of this, experiment was several months over which results were collected from numerous trials. As such it would be over exhaustive and under informative to present them on an individual trial by trial basis. Instead we present results in broad categories 1, 2, and 3 representing generally early (unsuccessful) runs, intermediate (semi-successful) runs, and later (ideally successful runs) explaining what went right and what went wrong in each, and how those issues were addressed in future runs.

## 5.1 Trial 1

Early trials took place within the first few months of the project timeline. These trials were about obtaining preliminary data and getting a feel on how the experiment was running and where potential improvements could be made. It was here that initial alignment was shown to be potentially inadequate as our SLM screen was not being projected faithfully onto our camera. Troubleshooting the issue unveiled 2 potential issues: the stability of both the optical mount the laser and heatsink were mounted on and potential synchronization issues.

The first issue became evident when beam drift was observed in our laser, which led to minimal light being transmitted through the optical components to our SLM, and what light was being propagated being woefully off-center on the SLM focal plane. The first being a hardware problem, it was necessary to change out the initial mount for a sturdier one, which subsequently required a ~10hr realignment of the entire system. The second presented a potentially more difficult issue that could potentially be addressed a number of ways, either in software or in hardware. In addition, a more careful perusal of relevant literature [vkoop thesis] revealed that synchronization was indeed an issue Velekoop and associates had encountered and addressed via complex timing mechanisms within their system.

Results for Intensity improvement and Enhancement factor gain were negligible at best in this stage and showed no real discernable data upon which to work with, suggesting serious issues in the implementation and execution of the experiment. On the positive note however, difficulties in early trials were extremely informative in providing soft data for properly executing this particular experiment.

## 5.2. Trial 2

These trials were characterized by moderate success by addressing some of the issues present in earlier trials, namely synchronization. As described in Chapter 4\_section 3 our initial plan was to implement a hardware synchronization loop via an MCX cable a simpler, almost trivial, software workaround was implemented instead via the use of the **pause()** function in MATLAB. Using the **pause()** function allowed us to circumvent exact synchronization in favor of a good-enough approximation. As opposed to trying to trigger the most possible times per unit time, we induce a delay to simply capture what necessary. The SLM refresh rate is approximately 60Hz plus a relaxation and stabilizing period for the liquid crystals within it. To address this we added a 150ms delay after each successive phase updating procedure. This adds approximately 1.5 seconds to each iteration, which is small but nontrivial in longer trials. It is a sacrifice of speed for overall functionality.

The other change made during these intermediate trials was to alter our method for projecting to the SLM. Initially we made use of a function **sendToProjectorRGB(X)** which allowed us to project a MATLAB generated matrix to the SLM surface via an extended monitor on PC. All phase values would be sent as the variable **X** to the function. One of the difficulties with **sendToProjectorRGB(X)**, was that as the second PC monitor was projected off-screen it was very difficult to monitor the position of the phase projected, as well as the updating process. In lieu of **sendToProjectorRGB(X)** the Holoeye Software Development Kit for the Pluto-2 was used to project our phase values. A more in depth description of how it increased functionality can be found in Section 4.6.

For these intermediate runs we used a 256 x 256 pixel region of our SLM broken into segments of size 16 x 16 giving us 256 phase updating iterations. We define our Area Of Interest as a 4x4 pixel directly in the center of our 400 x 400 camera plane. Quantitatively we saw an increase in intensity in our defined Area Of Interest leading to an overall enhancement factor gain of around 8 which plateaued after approximately 150 iterations. Qualitatively however; we did not observe a definitive intensity increase in the designated Area Of Interest, making this only a semi-successful trial period, but an improvement nonetheless.

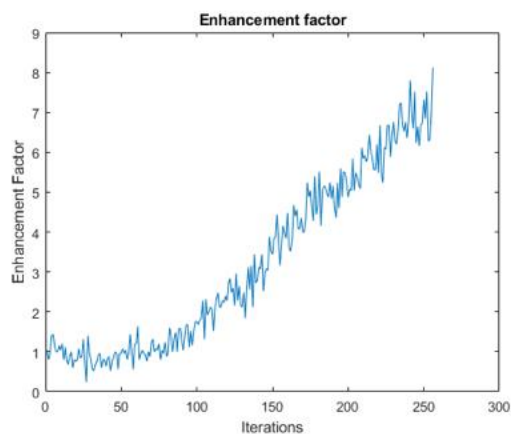


Fig. 14 a ) Enhancement Factor for Run 06-05

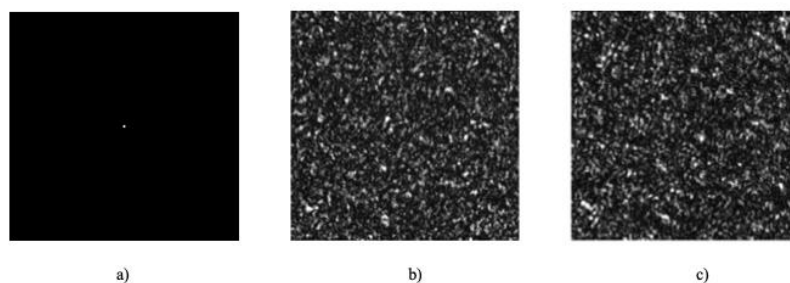


Fig. 15 a ) ROI Mask(Area of Interest) b) Initial Image for Run 06-05  
c) Final Image for Run 06-05

### 5.3 Trial 3

For our late stage trials, we strived to build on the earlier moderate successes of the intermediate runs. It appeared the concept was sound, but the execution could be improved with some changes. Our first change was to make micro adjustments to the alignment of our optical system to ensure enough power from our laser was reaching our camera plane by minimizing dissipation through our other optical elements. The result of this alignment allowed us to observe a small offset in the light reflecting off of the SLM which meant that anything projected on it would be represented slightly off-center and to the right in the camera plane. Realizing this, an offset was added to the relevant variables (discussed in Section 4.6) within the control program, which skewed our phase projection to the left to compensate for the right veering offset.

It was here that the use of the SDK for phase-projection became extremely useful. Through trial and error (use of a projected rectangular phase value on a black background) we were able to find approximately what the ideal offset should be. FIGURE below is the SLM screen post phase optimization, it is clear in the figure that our active region is not directly in the center.

The final adjustment was to increase the active area on the SLM to a 512 x 512 pixel region. This increased the number of phase addressable segments (and thus iterations) to 1024.

This trial overall was an overwhelming success. We again witnessed a significant intensity increase from initial conditions, as well as witnessing a huge enhancement factor gain.

Most, importantly we witnessed a visibly brighter spot in the defined Area of Interest. To analyze our results, we created an image which subtracted the intensities in the initial snapshot from the final snapshot. Observing this image in Fig. 17 it is obvious that a significant increase in intensity in our Area of Interest occurred. Additionally, a line plot of the intensities (as a 1D vector with) show an obvious peak directly in the center indices representing our Area of Interest.

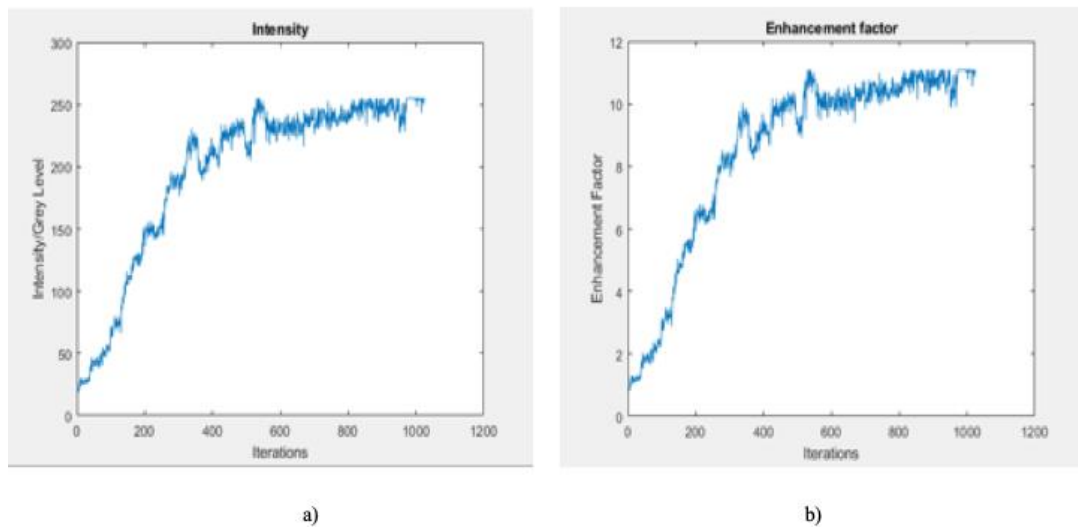


Fig. 16 a ) Intensity for 06-12 b) Final Image for Run 06-12

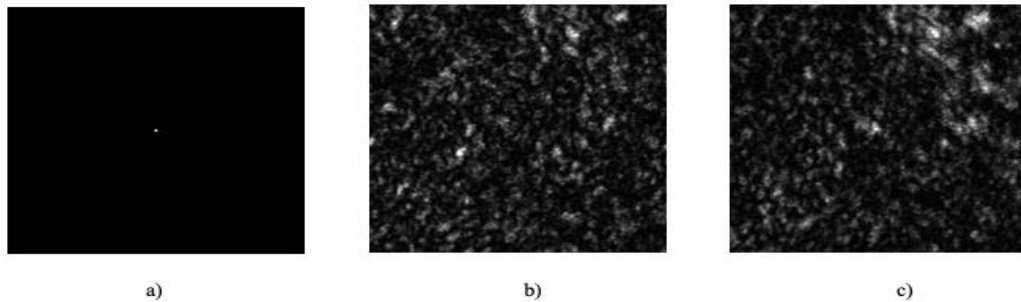


Fig. 17 a ) ROI Mask(Area of Interest) b) Initial Image for Run 06-12  
c) Final Image for Run 06-12

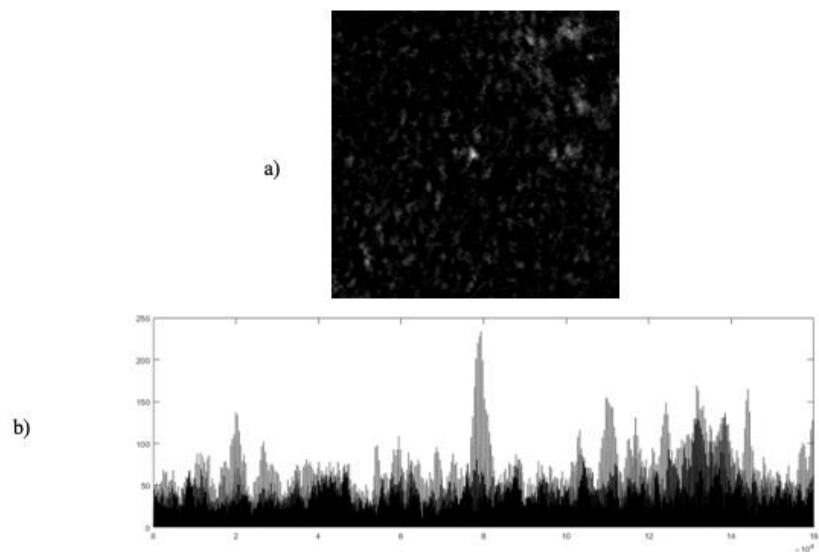


Fig. 18 a) (Final Image – Initial Image) Trial 06-12 b) Index Plot Trial 06-12

## CHAPTER 6. CONCLUSIONS & FUTURE WORK

The goal of this work was to implement focusing through scattering media partially as a proof of concept toward the achievement of imaging through scattering media. We have shown that we can optimize phase and drastically increase intensity in a small area of interest, equivalent to discovering a single eigenchannel of the transmission matrix. Imaging through scattering media involves optimizing phase for the entire media in order to propagate a full spatial intensity distribution (i.e. an image). This is equivalent to finding an approximation to all the eigenchannels through the media.

### 6.1 Future Work

#### **Machine Learning Based Algorithms**

The next potential work moving forward we would like to try and implement machine learning techniques into our experiment. Our method using optimization of phase to find the values of the transmission matrix through a scattering media. However, this type of procedure is highly susceptible to decorrelations in the speckle pattern— small perturbations to the scattering medium, such as those caused by vibrations, lead to errors and severe degradation of the imaging procedure. [38] The goal in their work is to develop a new framework that is highly scalable to both medium perturbations and measurement requirement. To do so, they propose a statistical ‘one-to-all’ deep learning technique that accounts for a wide range of statistical variations for the model to be resilient to speckle decorrelations. Another work [39] uses a data driven approach and leverages convolutional neural networks (CNN) to “learn a model that is invariant to calibration parameters variations within the training range and nearly invariant beyond that.” This will potentially allow the group to achieve robust, calibration independent imaging through scattering

media.

### **Computation via Wave Shaping**

While the use of Spatial Light Modulators to achieve wavefront shaping is rightfully bountiful in the optics domain, other researchers have begun to utilize its methodology and techniques in other areas as well. One of those areas is in computation. Computation in general is of particular interest to this researcher, and applications of alternative computing paradigms such as analog computation have become of particular interest as we near the limits of Moore's Law [40]. To that end, another potential future work is based on [41]. In this work P. Hougue et. al utilize wave-based computation to achieve a Discrete Fourier transform of a 16 x 16 complex valued image. They suggest that — subject to appropriate wavefront shaping — any disordered medium may in fact serve as reconfigurable computation unit. To achieve this, they utilize Wi-Fi waves reverberating in a room as their disordered media and phase reflect arrays to achieve computation by shaping these waves appropriately.

## REFERENCES

1. I. M. Vellekoop, *Controlling the propagation of light in disordered scattering media* (2008).
2. F. T.S.Yu, “Light and information,” *J. Appl. Opt.* **37**(6), 503–509 (2019) [doi:10.5768/jao201637.0601002].
3. J. M. Schmitt and G. Kumar, “Optical scattering properties of soft tissue: a discrete particle model,” *Appl. Opt.* **37**(13), 2788 (2008) [doi:10.1364/ao.37.002788].
4. S. H. Simon et al., “Communication in a disordered world,” *Phys. Today* **54**(9), 38–43 (2001) [doi:10.1063/1.1420510].
5. C. F. Bohren and D. R. Huffman, *Absorption and scattering of light by small particles*, Wiley, New York (1983).
6. E. M. Eyring, *Topics in Applied Physics*, in *Nuclear Technology* **39**(3) (2017) [doi:10.13182/nt78-a32063].
7. B. Gerardin et al., “Particle-like wave packets in complex scattering systems,” 2016 URSI Int. Symp. Electromagn. Theory, EMTS 2016 **014209**, 265–268 (2016) [doi:10.1109/URSI-EMTS.2016.7571370].
8. J. H. Li and A. Z. Genack, “Correlation in laser speckle,” *Phys. Rev. E* **49**(5), 4530–4533 (1994) [doi:10.1103/PhysRevE.49.4530].
9. O. S. Ojambati et al., “Mapping the energy density of shaped waves in scattering media onto a complete set of diffusion modes,” *Opt. Express* **24**(16), 18525 (2016) [doi:10.1364/oe.24.018525].
10. R. E. Parks, “Alignment of optical systems,” *Int. Opt. Des. Conf. 2006* **6342**(September), 634204 (2006) [doi:10.1117/12.692190].
11. I. M. Vellekoop and A. P. Mosk, “Phase control algorithms for focusing light through turbid media,” 3071–3080 (2008) [doi:10.1016/j.optcom.2008.02.022].
12. B. Coyotl-Ocelotl et al., “Implementation of focusing and redirecting light through highly scattering media,” *SPECKLE 2015 VI Int. Conf. Speckle Metrol.* **9660**(August 2015), 96601X (2015) [doi:10.1117/12.2202820].
13. A. P. Mosk et al., “Controlling waves in space and time for imaging and focusing in complex media,” *Nat. Photonics* **6**(5), 283–292 (2012) [doi:10.1038/nphoton.2012.88].

14. A. P. Mosk and I. M. Vellekoop, “Focusing coherent light through opaque strongly scattering media,” *Opt. Lett.* **32**(16), 2309–2311 (2007).
15. A. Saade et al., “Random projections through multiple optical scattering: Approximating Kernels at the speed of light,” *ICASSP, IEEE Int. Conf. Acoust. Speech Signal Process. - Proc.* **2016-May**, 6215–6219 (2016) [doi:10.1109/ICASSP.2016.7472872].
16. zhuang bin et al., “Imaging through a scattering medium based on spatial transmission matrix,” *10* (2017) [doi:10.1117/12.2285014].
17. M. C. Tropicarsky et al., “Transfer-matrix formalism for the calculation of optical response in multilayer systems: from coherent to incoherent interference,” *Opt. Express* **18**(24), 24715 (2010) [doi:10.1364/oe.18.024715].
18. P. Kužel, “Layered structures : transfer matrix formalism.”
19. F. Dolcini, “Introduction to the Scattering Matrix Formalism,” *Lect. Notes XXIII Phys. GradDays(October)*, 5–9 (2009).
20. N. Konforti, E. Marom, and S.-T. Wu, “Phase-only modulation with twisted nematic liquid-crystal spatial light modulators,” *Opt. Lett.* **13**(3), 251 (2008) [doi:10.1364/ol.13.000251].
21. M. C. W. van Rossum and T. M. Nieuwenhuizen, “Multiple scattering of classical waves: microscopy, mesoscopy, and diffusion,” *Rev. Mod. Phys.* **71**(1), 313–371, American Physical Society (1999) [doi:10.1103/RevModPhys.71.313].
22. E. Akkermans and G. Montambaux, *Mesoscopic Physics of Electrons and Photons*, Cambridge University Press, Cambridge (2007) [doi:DOI: 10.1017/CBO9780511618833].
23. J. X. Zhu, D. J. Pine, and D. A. Weitz, “Internal reflection of diffusive light in random media,” *Phys. Rev. A* **44**(6), 3948–3959, American Physical Society (1991) [doi:10.1103/PhysRevA.44.3948].
24. S. Chandrasekhar, *Radiative transfer*, Dover Publications, New York (1960).
25. O. N. Dorokhov, *Solvable model of multichannel localization*, in *Physical review. B, Condensed matter* **37** (1988) [doi:10.1103/PhysRevB.37.10526].
26. V. P. Tishkovets, E. V. Petrova, and M. I. Mishchenko, “Scattering of electromagnetic waves by ensembles of particles and discrete random media,” *J. Quant. Spectrosc. Radiat. Transf.* **112**(13), 2095–2127 (2011) [doi:10.1016/j.jqsrt.2011.04.010].

27. P. M. Morse and H. Feshbach, *Methods of Theoretical Physics* (McGraw-Hill, 1953).
28. C. A. M and C. Miniatura, “Multiple scattering of light by atoms with internal,” *Online* **35**, 10163–10188 (2002).
29. C. W. J. Beenakker, “RMP69-731.pdf,” 731–808 (1997).
30. C. Gong, “Total variation optimization for imaging through turbid media with transmission matrix” (2019) [doi:10.1117/1.OE.55.12.121703].
31. M. I. Mishchenko et al., *T-matrix theory of electromagnetic scattering by particles and its applications: A comprehensive reference database*, in *Journal of Quantitative Spectroscopy and Radiative Transfer* **88**(1–3) (2004) [doi:10.1016/j.jqsrt.2004.05.002].
32. P. M. Page, *Liquid Crystals Tomorrow*, in *Liquid Crystals Today* **9**(2) (2007) [doi:10.1080/13583149908047724].
33. P. Raynes, “LIQUID CRYSTALS — Second Edition, by S CHANDRASEKHAR, Cambridge University Press, (1992), ISBN 0-521-41747-3 (HB), ISBN 0-521-42741-X (PB),” *Liq. Cryst. Today* **3**(3), 7, Taylor & Francis (1993) [doi:10.1080/13583149308628627].
34. P. G. DeGennes, *The Physics of Liquid Crystals*, 2nd ed., Clarendon Press, Oxford (1974).
35. G. Lazarev et al., *LCOS spatial light modulators: Trends and Applications*, in *Optical Imaging and Metrology: Advanced Technologies* (August) (2012) [doi:10.1002/9783527648443.ch1].
36. M. Coherent, “Operator’s Manual Coherent,” Control.
37. “Camera Models and Parameters.”
38. Y. Li, Y. Xue, and L. Tian, “Deep speckle correlation: a deep learning approach toward scalable imaging through scattering media,” *Optica* **5**(10), 1181–1190, OSA (2018) [doi:10.1364/OPTICA.5.001181].
39. G. Satat et al., “Object classification through scattering media with deep learning on time resolved measurement,” *Opt. Express* **25**(15), 17466 (2017) [doi:10.1364/oe.25.017466].
40. Y. Huang et al., “Analog Computing in a Modern Context: A Linear Algebra Accelerator Case Study,” *IEEE Micro* **37**(3), 30–38 (2017) [doi:10.1109/MM.2017.55].

41. P. Del Hougne and G. Lerosey, "Leveraging Chaos for Wave-Based Analog Computation: Demonstration with Indoor Wireless Communication Signals," *Phys. Rev. X* **8**(4) (2018) [doi:10.1103/PhysRevX.8.041037].
42. I.M. Optics, "Why Choose Meadowlark's Reflective SLMs?", *Meadowlark.com*, 2019, <<https://www.meadowlark.com/why-choose-meadowlark-39-reflective-slms-p-123?mid=17>>